Asian Journal of Chemistry; Vol. 38, No. 2 (2026), 308-322
ASIAN JOURNAL OF CHEMISTRY
https://doi.org/10.14233/ajchem.2026.34691

Synthesis, Characterisation and *in silico* Evaluation of Imidazole-Based Schiff Base Transition Metal(II) Complexes with Antioxidant and Antidiabetic Potential

M.B. MANU[1], P. DEEPIKA[2], N. SRIKANTAMURTHY[3], H.M. VINUSHA[4], S.M. MADAN[2] and K.B. UMESHA[1,*]

[1]Department of Chemistry, Yuvaraja College, University of Mysore, Mysuru-570005, India
[2]Department of Chemistry, JSS Science and Technology University, Mysuru-570006, India
[3]Department of Chemistry, Vidyavardhaka College of Engineering, Visvesvaraya Technological University, Mysuru-570005, India
[4]Post-Graduate Department of Chemistry, Sarada Vilas College, Mysuru-570004, India

*Corresponding author: E-mail: kbu68umesha@gmail.com

Received: 14 August 2025 *Accepted*: 30 November 2025 *Published online*: 31 January 2026 AJC-22249

In this work, few transition metal(II) complexes of Cu^{2+}, Co^{2+}, Ni^{2+} and Zn^{2+} were synthesised with imidazole-based Schiff base ligand, (*E*)-*N*-(4-chlorobenzo[*d*]thiazol-2-yl)-1-(1*H*-indole-3-yl)methanimine. These complexes were characterised by mass, NMR and FT-IR spectroscopies. The NMR and FT-IR spectral data confirmed coordination of the azomethine nitrogen and sulphur atoms with the metal centers. The physico-chemical properties, drug-likeness parameters and pharmacokinetic behaviour of the imidazole-based Schiff base ligand and its metal(II) complexes were predicted using the SwissADME web server. Bioactivity prediction and PASS analysis further validated the favourable drug-like characteristics of both the free ligand and its metal(II) complexes. Molecular docking studies were carried out using AutoDock Vina against selected biological targets, including an antioxidant enzyme (PDB ID: 1HD2), ferritin (PDB ID: 1FHA) and α-amylase (PDB ID: 2QV4). The docking results demonstrated strong binding affinities and significant intermolecular interactions with the active sites of the target proteins, thereby supporting the multifunctional therapeutic potential of the synthesized metal complexes. Notably, the compounds exhibited pronounced antioxidant and antidiabetic activities, underscoring their promise as effective bioactive agents. Overall, these findings suggest that the synthesized Schiff base metal(II) complexes represent promising candidates for further development as multifunctional therapeutic agents.

Keywords: Schiff base ligand, Pharmacokinetics, Bioactivity, Antioxidant activity, Antidiabetic activity, Drug-likeness evaluation.

INTRODUCTION

Coordination chemistry has gained significant attention in recent years, in part due to its potential in developing more effective, targeted and safer metal-based medications for nutritional and metabolic applications [1]. A defining feature of coordination compounds is the unique arrangement of ligands around the central metal ion. These compounds are fundamentally composed of metals, ligands and their interactions [2]. Schiff bases, in particular, exhibit enhanced activity when they form complexes with transition metals, making them vital in a variety of applications [3-5].

In coordination compounds, transition metal ions serve as crucial central metal centers. The biological activity and applications of these compounds are strongly influenced by the nature of both the metal ions and the ligands involved. As a result, coordination compounds have found diverse applications, including oxygen carriers, metalloenzymes, catalysts and sensors [6-8]. Furthermore, metal complexes have been extensively studied for their therapeutic potential, particularly in the treatment of diabetes, bacterial and fungal infections and tumors [9,10].

There is a continuous effort to explore and design new transition metal complexes to enhance their biological applications. This research remains a thriving and crucial field within bio-inorganic chemistry. The selection of ligands, in conjunction with metal ions, is critical in determining the properties and effectiveness of these complexes [11,12]. Over the years, Schiff base ligands have become particularly attractive, with their metal complexes being rapidly developed, especially for their therapeutic potential [13]. Such metal complexes are increasingly recognised in the fields of phar-

macology due to their antifungal, antibacterial, antitumor and anticarcinogenic properties [14,15]. Based on the diverse applications and the promising biological and chemical properties of Schiff base metal complexes discussed above, a novel Schiff base ligand, *N*-(4-chlorobenzo[*d*]thiazol-2-yl)-1-(1*H*-indole-3-yl)methenamine, was synthesized along with its corresponding metal(II) complexes incorporating Cu(II), Co(II) Ni(II) and Zn(II) ions. The ligand and its metal complexes were designed to systematically investigate their biological and chemical potential, with the objective of enhancing their effectiveness for drug development and therapeutic applications.

EXPERIMENTAL

2-Amino-4-chlorobenzothiazole (≥ 99% purity, CAS No. 19952-47-7) and 2-imidazolecarboxyaldehyde (≥ 99% purity, CAS No. 10111-08-7) were sourced from Sigma-Aldrich and used as received. All the metal salts and solvents, purchased from E. Merck, were also used directly without purification.

Thin layer chromatography (TLC) was performed on pre-coated silica gel plates (Merck, India) to monitor the reaction progress. The carbon, hydrogen, nitrogen and sulphur contents of the metal(II) complexes was determined using a CHNS elemental analyzer. The metal contents were quantified using atomic absorption spectroscopy (AAS) on a Perkin-Elmer AAnalyst 400 instrument after acid digestion of the samples in a mixture of HNO_3 and HCl (aqua regia). Calibration was performed using standard metal solutions of known concentrations. Infrared spectra were recorded on a Perkin-Elmer FT-IR 1650 spectrophotometer using KBr pellet method. The spectra were recorded in the range of 4000-400 cm^{-1} in transmittance mode. The measurements were conducted using a DTGS detector and a KBr beamsplitter, which is suitable for the mid-IR region. ^{1}H NMR spectra were obtained on a Varian 300 MHz spectrometer with DMSO-d_6 as the solvent and tetramethylsilane as the internal standard. Mass spectra were acquired using an Agilent Technologies (HP) 5973 mass spectrometer with an ionisation potential of 70 eV.

Synthesis of Schiff base ligand *N*-(4-chlorobenzo[*d*]-thiazol-2-yl)-1-(1*H*-indole-3-yl)methenamine: Equimolar quantities of 2-amino-4-chlorobenzothiazole and 2-imidazolecarboxaldehyde were dissolved in methanol in a clean, dry flask. A few drops of acetic acid were added to facilitate the condensation reaction. The reaction mixture was stirred at room temperature and then heated to 50-60 ºC. Stirring was continued for 8 h and the progress of the reaction was monitored by TLC. Upon completion, the reaction mixture was cooled to room temperature and then gradually added to ice-cold water, resulting in the precipitation of the Schiff base product. The precipitate was filtered, washed with cold water to remove unreacted materials and byproducts and then dried at room temperature or under reduced pressure (**Scheme-I**).

Synthesis of metal(II) complexes: A general synthetic procedure was adopted for the preparation of the metal(II) complexes by reacting the corresponding chloride salts of Cu^{2+}, Co^{2+}, Ni^{2+} and Zn^{2+} with the Schiff base ligand. The metal salts were initially dissolved in ethanol, after which the Schiff base ligand was introduced in a metal-to-ligand molar ratio of 1:2. The metal salt solution was added dropwise to the ligand solution under continuous magnetic stirring. The reaction mixture was then stirred at room temperature for 1 h to ensure complete complexation. Upon completion of the reaction, the resulting solid metal complexes were collected by filtration, washed thoroughly with ethanol to remove unreacted species and finally dried in an oven at 50 ºC to eliminate the residual solvent.

***In silico* drug-likeness, ADMET and BOILED-egg model analysis:** The physico-chemical properties and drug-likeness of the Schiff base ligand and its metal(II) complexes were evaluated using several online tools. The SwissADME model was used to calculate the physico-chemical properties and drug-likeness scores, as well as to analyze the boiled egg images of the ligand and its metal(II) complexes. Moreover, the Molsoft LLC website (https://www.molsoft.com/mprop/) was employed to calculate the drug-likeness scores [16]. Standard pharmacokinetic parameters including absorption, distribution, metabolism and excretion (ADME), were analysed to estimate their potential for drug discovery. To assess toxic properties, the ADMET Lab 2.0 tool (https://admetmesh.scbdd.com/service/evaluation/cal) and the pkCSM online tool were used to predict ADMET (absorption, distribution, metabolism, excretion and toxicity) properties [17,18].

Prediction of activity spectra for substances (PASS): Prediction of Activity Spectra for Substances (PASS) analysis was performed to evaluate the potential biological activities of the synthesized ligand and its metal(II) complexes based on their chemical structures. The PASS algorithm predicts a biological activity spectrum, which represents the probable biological functions of a compound arising from its interactions with biological systems. This spectrum was used as the computational basis for assessing the likely bioactivities of the investigated compounds [19,20].

Molecular docking: Molecular docking of the synthesised Schiff base ligand and its metal(II) complexes was conducted using AutoDock Vina, a computational docking

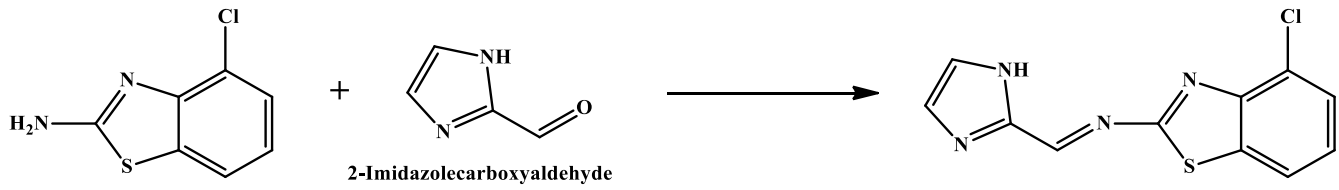

2-Amino-4-chlorobenzothiazole + **2-Imidazolecarboxyaldehyde** → **(*E*)-*N*-(4-Chlorobenzo[*d*]thiazol-2-yl)-1-(1*H*-imidazol-2-yl)methanimine**

Scheme-I: Synthesis of imidazole-based Schiff base ligand

program. The protein structures were obtained from the RCSB Protein Data Bank. The selected proteins included an antioxidant protein (PDB ID: 1HD2), ferritin (human ferritin heavy chain; PDB ID: 1FHA) and a diabetes-related protein, mammalian pancreatic α-amylase (PDB ID: 2QV4). The aim of the study was to predict the interactions between the compounds and the proteins.

The compounds and proteins were prepared using AutoDock Tools by adding charges, assigning atom types, setting macromolecules and defining ligands as map types. Both the ligands and protein structures were saved in PDBQT format. Further processing of the protein structures was carried out in Discovery Studio 2021, where bound ligands and water molecules were removed and polar hydrogens were added. Docking simulations were then performed using AutoDock Vina and the resulting binding interactions were analysed using Discovery Studio [20,21].

In vitro biological activities

Antioxidant activity

Ferric reducing antioxidant power (FRAP): The ferric reducing antioxidant power (FRAP) assay was performed to evaluate the antioxidant capacity of the studied compounds. The FRAP approach, which is based on reducing the Fe^{3+}–TPTZ complex to the Fe^{2+}–TPTZ complex in the presence of antioxidants, was used to evaluate the antioxidant capabilities of the compounds. Briefly, 100 µL of the stock solution of each compound or the blank (DMSO) was transferred into a test tube, followed by the addition of 3 mL of freshly prepared FRAP reagent containing 2,4,6-tripyridyl-s-triazine (TPTZ), $FeCl_3$ and acetate buffer (pH 3.6). The reaction mixtures were incubated at 37 ºC for 4 min, after which the absorbance was recorded at 593 nm using a UV-Vis spectrophotometer [22]. Blank samples containing only the FRAP reagent were analyzed simultaneously and the final absorbance values were obtained by subtracting the corresponding blank readings from the sample absorbance. Antioxidant capacity was quantified using a calibration curve constructed with $FeSO_4·7H_2O$ in the concentration range of 31.25-1000 µM. The results were expressed as µM $FeSO_4·7H_2O$ equivalents per gram of compound [23].

DPPH radical-scavenging activity: The free radical scavenging activity of the synthesized compounds was evaluated using the 2,2-diphenyl-1-picrylhydrazyl (DPPH) assay. Stock solutions of the compounds were prepared in DMF and diluted to obtain final concentrations of 100, 200, 300, 400 and 500 µg/mL. For each concentration, 1 mL of compound solution was mixed with 1 mL of methanolic DPPH solution and incubated in the dark at room temperature for 30 min. Ascorbic acid was used as the reference standard. After incubation, the absorbance of the reaction mixtures and the control was measured at 517 nm using a UV-Vis spectrophotometer [24]. All experiments were performed in triplicate and the results were expressed as mean ± standard deviation. The percentage of DPPH radical scavenging activity was calculated using the following equation:

$$\text{Inhibition (\%)} = \frac{A_{control} - A_{sample}}{A_{control}} \times 100$$

ABTS radical scavenging: The ABTS radical cation scavenging activity of the Schiff base ligand and its metal(II) complexes was evaluated using the ABTS assay. The $ABTS^{•+}$ stock solution was prepared by mixing equal volumes (1:1) of 7 mM ABTS solution and 2.4 mM potassium persulfate solution, followed by incubation at room temperature for 12 h in dark to allow complete radical generation. The resulting $ABTS^{•+}$ solution was subsequently diluted with distilled water to obtain an absorbance of approximately 0.70 ± 0.02 at 734 nm. In brief, 1 mL of the test sample solution was mixed with 1 mL of the diluted $ABTS^{•+}$ solution, and the reaction mixture was allowed to stand at room temperature. The decrease in absorbance was recorded at 734 nm using a UV-Vis spectrophotometer. Ascorbic acid was used as the reference standard and its radical scavenging activity was compared with that of the Schiff base ligand and the corresponding metal(II) complexes. All measurements were carried out in triplicate and the results were expressed as mean values. The following formula was used to determine the percentage inhibition of ABTS radical scavenging activity:

$$\text{Inhibition (\%)} = \frac{Abs_{control} - Abs_{sample}}{Abs_{control}} \times 100$$

where $Abs_{control}$ = absorbance of $ABTS^{•+}$ + DMF and Abs_{sample} = absorbance of $ABTS^{•+}$ + sample [test samples/standard]

Antidiabetic activity (α-amylase inhibitory assay): The 3,5-dinitrosalicylic acid (DNSA) method was used to determine the percentage of α-amylase inhibition (%) using acarbose as a standard. The inhibitory activity of α-amylases was calculated as a percentage of inhibition using the following formula:

$$\text{Inhibition (\%)} = \frac{A_{control} - A_{sample}}{A_{control}} \times 100$$

The IC_{50} values were determined by plotting the percentage of inhibition against the corresponding concentrations of each test sample. All experiments were performed in triplicate with appropriate blanks included. The IC_{50} value was defined as the concentration of the compound required to inhibit 50% of α-glucosidase activity under the specified experimental conditions [25,26].

RESULTS AND DISCUSSION

The synthesis of the Schiff base ligand (*E*)-*N*-(4-chlorobenzo[*d*]thiazol-2-yl)-1-(1*H*-indole-3-yl)methanimine is outlined in **Scheme-I**. The proposed molecular structures of the corresponding Cu(II), Co(II), Ni(II), and Zn(II) complexes derived from this ligand are depicted in Fig. 1. The coordination modes and bonding interactions illustrated are proposed on the basis of spectroscopic evidence and by analogy with structurally related Schiff base metal complexes reported in the literature. Although single-crystal X-ray diffraction data were not obtained, the suggested coordination geometries are consistent with previously reported structures for comparable metal-Schiff base systems [27,28].

All the synthesized compounds are stable at room temperature but decompose when heated to temperatures above

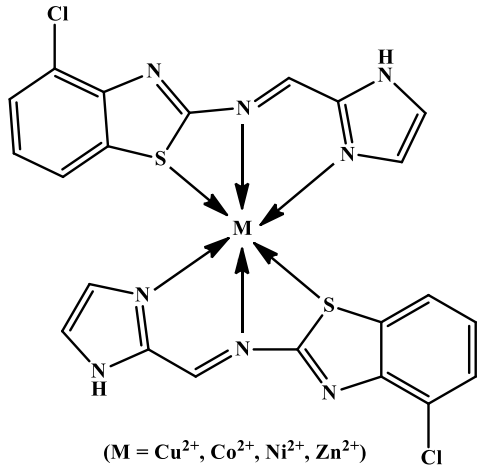

Fig. 1. Proposed structure of Schiff base metal(II) complexes

200 ºC. All the compounds were found to be nearly insoluble in water, with solubility varying across different organic solvents. Table-1 presents the elemental analysis of the Schiff base ligand and its metal(II) complexes, showing good agreement with the calculated values. The stoichiometry of the Schiff base ligand and its metal(II) complexes was confirmed through elemental analysis.

Mass spectral studies: Mass spectrometry was employed to confirm the formation of the ligand and its metal(II) complexes. Fig. 2 displays the mass spectrum of the Schiff base ligand, with a molecular ion peak at *m/z* 261.16, confirming its successful synthesis. The mass spectra of the metal(II) complexes with Cu^{2+}, Co^{2+}, Ni^{2+} and Zn^{2+} ions. The molecular ion peaks observed at *m/z* 586.17 for the Cu(II) complex, *m/z* 581.00 for the Co(II) complex, *m/z* 581.20 for the Ni(II) complex and *m/z* 587.71 for the Zn(II) complex strongly indicate the coordination of the ligand with these metal ions. These peaks align with the predicted empirical formulas, further validating the identity and structural integrity of both the ligand and its metal(II) complexes. The additional peaks present in the mass spectra of both the ligand and its metal(II) complexes are its fragmentation products.

NMR spectral studies: Fig. 3a shows the ^{1}H NMR spectrum of the Schiff base ligand recorded in DMSO solvent. A prominent signal at δ 9.655 ppm corresponds to the azomethine group (HC=N), a characteristic feature of the Schiff base ligand. The spectrum also displays multiplet signals for the aromatic protons in the range of δ 6.974-7.850 ppm. Moreover, a singlet peak at δ 13.585 ppm is observed for the NH group of the imidazole moiety. These signals collectively confirm the successful synthesis of the Schiff base ligand [29,30].

Fig. 3b shows the ^{13}C NMR spectrum of the Schiff base ligand recorded in DMSO solvent. A prominent signal at δ 166.71 ppm is attributed to the azomethine group, a characteristic feature of the Schiff base ligand. The spectrum also displays multiplet signals for the aromatic carbons in the range of δ 108.39-152.36 ppm. The signal at δ 169.64 ppm is attributed to the carbon of the benzothiazole ring. These peaks confirm the formation of the Schiff base ligand [31,32]. The ^{13}C NMR spectra show the minor signals attributable to trace impurities, possibly residual solvents.

Infrared spectral studies: Fig. 4 shows the FT-IR spectra of Schiff base ligand (L) and its metal(II) complexes. The FT-IR spectrum of the Schiff base ligand (L) shows characteristic absorption bands and is summarised in Table-2. The IR spectrum of the Schiff base ligand (peak 1) displayed a strong absorption peak at 1647 cm^{-1}, corresponding to the stretching vibration of the azomethine group (HC=N). The peak at 1534 cm^{-1} corresponds to stretching vibrations of C=C. The absorption band at 620 cm^{-1} corresponds to stretching vibrations of C–Cl group. Moreover, a peak around 3045 cm^{-1} were observed, indicating the presence of aromatic C–H stretching vibrations. These stretching frequencies support the formation of a ligand.

In contrast, the IR spectra of the metal(II) complexes showed notable changes. The formation some new bands at specific frequencies confirms the formation of ligand metal coordinate bond. The HC=N stretching vibration shifted to the lower frequencies, indicating coordination between the Schiff base ligand and its metal(II) ion. The stretching vibrations at 534 cm^{-1} and 423 cm^{-1} corresponds to the ν(Cu–S) and ν(Cu–N) metal bonds, respectively. These spectral changes confirm the successful coordination of the Schiff base ligand with the metal ions, providing valuable insights into the structure of the complexes [33,34]. The appearance of new bands at these stretching frequencies were taken as an on indication of coordination between the metal ions and nitrogen and sulphur. Similarly, for other metal(II) complexes, the key IR stretching vibrations are shown in Table-2.

***In silico* drug-likeness, ADMET and BOILED-egg model analysis:** The *in silico* pharmacokinetic and toxicity

TABLE-1
PHYSICO-CHEMICAL DATA OF IMIDAZOLE-BASED SCHIFF BASE LIGAND AND ITS METAL(II) COMPLEXES

Compounds	m.f.	Colour	m.w.	m.p. (ºC)	Yield (%)	Elemental analysis (%): Found (calcd.)					
						C	H	Cl	M	N	S
Schiff base ligand	$C_{11}H_7N_4SCl$	Cream	261.16	235.00	89	50.29 (49.85)	2.69 (2.57)	13.49 (13.04)	–	21.33 (20.68)	12.20 (12.06)
Cu(II) complex	$C_{22}H_{14}CuN_8S_2Cl_2$	Blue	586.17	283.16	76	44.86 (43.12)	2.40 (2.51)	12.04 (12.15)	10.79 (10.27)	19.03 (18.24)	10.89 (10.24)
Co(II) complex	$C_{22}H_{14}CoN_8S_2Cl_2$	Reddish-brown	581.00	239.67	81	45.22 (46.28)	2.41 (2.35)	12.13 (11.99)	10.09 (9.89)	19.18 (19.24)	10.97 (11.01)
Ni(II) complex	$C_{22}H_{14}NiN_8S_2Cl_2$	Light green	581.20	228.43	69	45.24 (44.19)	2.42 (2.47)	12.14 (11.91)	10.05 (9.97)	19.18 (18.99)	10.98 (11.05)
Zn(II) complex	$C_{22}H_{14}ZnN_8S_2Cl_2$	Pale yellow	587.71	248.44	72	44.73 (45.08)	2.39 (2.31)	12.00 (12.06)	11.07 (10.81)	18.97 (18.79)	10.85 (10.35)

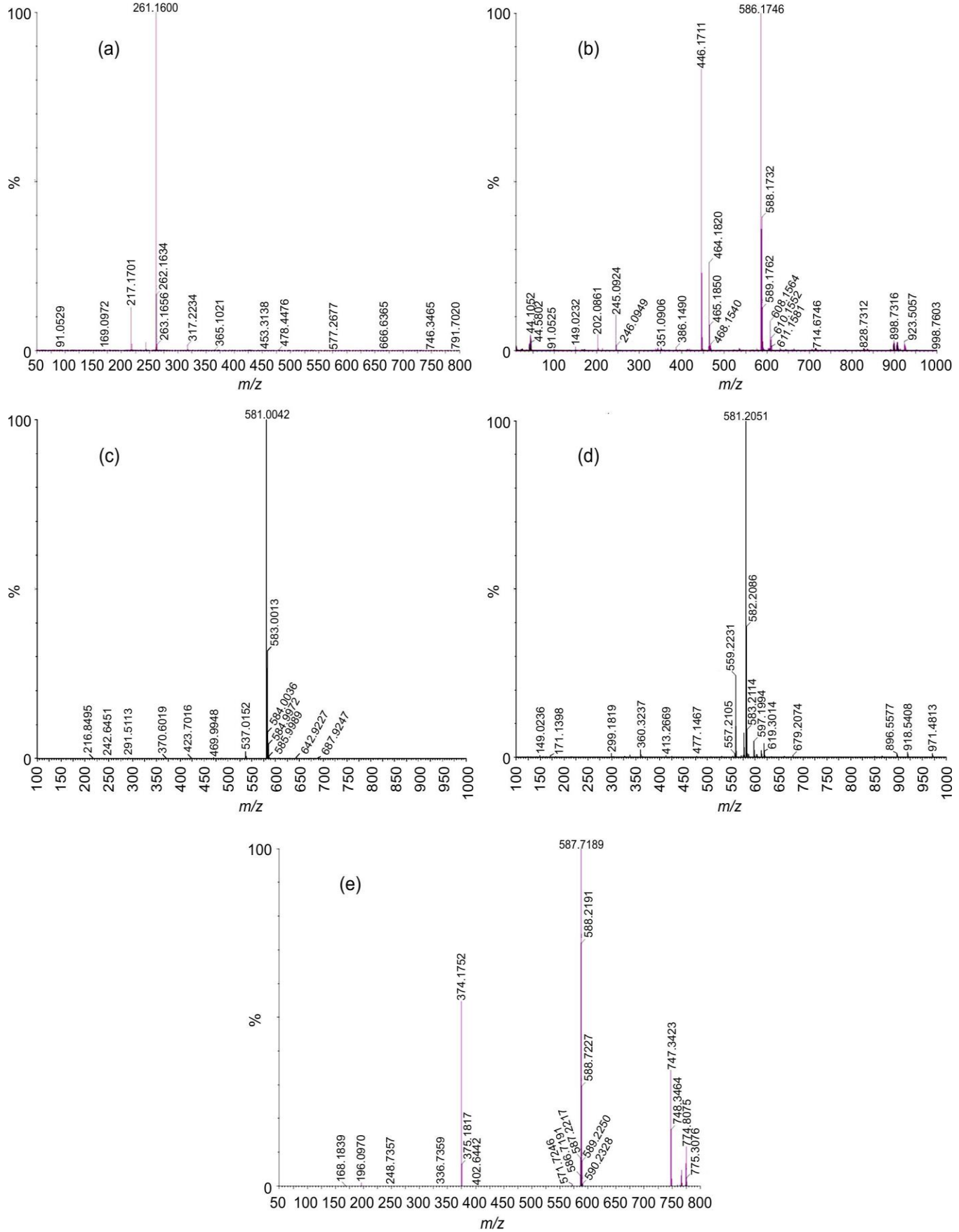

Fig. 2. Mass spectra of (a) imidazole-based Schiff base ligand, (b) Cu(II) (c) Co(II), (d) Ni(II) and (e) Zn(II) complexes

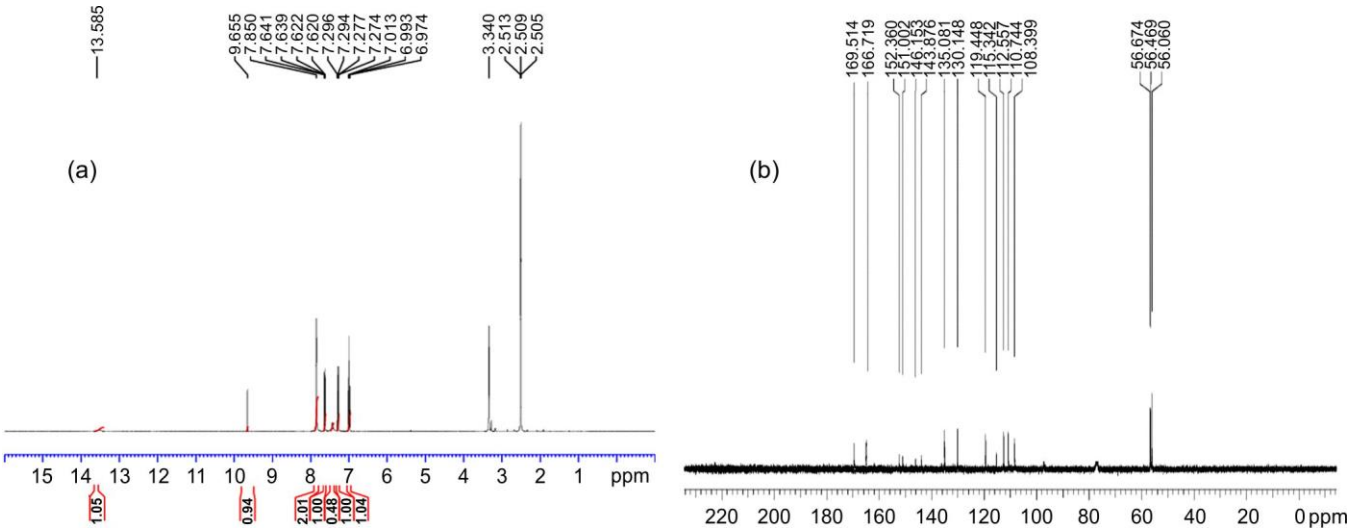

Fig. 3. ^{1}H NMR (a) and ^{13}C NMR (b) spectra of imidazole-based Schiff base ligand

TABLE-2
FT-IR CHARACTERISTIC PEAKS FREQUENCIES OF IMIDAZOLE-BASED SCHIFF BASE LIGAND AND ITS METAL(II) COMPLEXES (cm^{-1}) CORRESPONDING TO STRETCHING VIBRATIONS

Compound	C–H	HC=N	C=C	C–Cl	M–S	M–N
Schiff base ligand	3045	1652	1540	680	–	–
Cu(II) complex	3105	1635	1523	629	534	423
Co(II) complex	3071	1695	1548	689	585	439
Ni(II) complex	3002	1609	1521	606	531	463
Zn(II) complex	3028	1608	1523	697	559	491

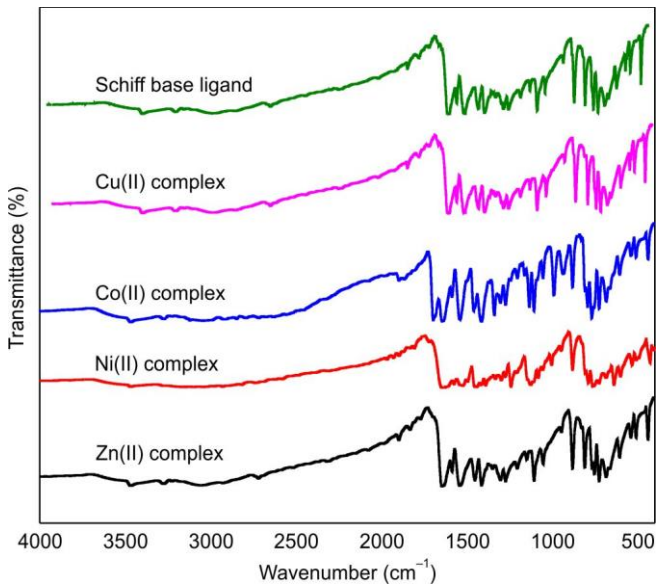

Fig. 4. IR spectra of Schiff base ligand and its metal(II) complexes

profiles of the Schiff base ligand and its Cu(II), Co(II), Ni(II), and Zn(II) complexes were evaluated using the pkCSM tool, and the predicted ADMET parameters are summarized in Table-3. Overall, the results indicate that both the free ligand and its metal(II) complexes exhibit favourable drug-likeness and pharmacokinetic characteristics, supporting their potential as bioactive candidates. From the absorption perspective, all compounds showed acceptable intestinal absorption values, suggesting their suitability for oral administration. The predicted Caco-2 permeability and skin permeability values further indicate moderate membrane permeability, which is desirable for systemic bioavailability. Distribution parameters including volume of distribution and fraction unbound suggesting the adequate tissue distribution, while the blood-brain barrier (BBB) permeability predictions indicate limited central nervous system penetration for most metal(II) complexes, which is advantageous in minimizing potential neurotoxicity.

Metabolic profiling revealed that the Schiff base ligand and its metal(II) complexes are not predicted to act as substrates or inhibitors of key cytochrome P450 enzymes in most of the cases, indicating a reduced likelihood of adverse drug-drug interactions. The excretion-related parameters, particularly total clearance values, suggest reasonable elimination profiles without excessive accumulation. Importantly, toxicity predictions demonstrated the absence of AMES toxicity, hepatotoxicity and skin sensitization for the metal(II) complexes, further supporting their safety profile.

The bioavailability radar plots (Fig. 5) provide a visual summary of drug-likeness by integrating key physico-chemical descriptors such as lipophilicity, polarity, solubility, flexibility, size and saturation. The Schiff base ligand and its metal(II) complexes largely fall within the optimal ranges, indicating good drug similarity and balanced physico-chemical properties conducive to biological activity.

The BOILED-egg model (Fig. 6) was employed to assess passive gastrointestinal absorption and BBB permeation. In this model, the white region corresponds to a high probability of intestinal absorption, while the yellow “yolk” region indicates potential BBB penetration. The ligand was positioned

TABLE-3
ADME AND TOXICITY PREDICTION OF IMIDAZOLE-BASED SCHIFF BASE LIGAND AND ITS METAL(II) COMPLEXES

Parameters		Schiff base ligand	Cu(II) complex	Co(II) complex	Ni(II) complex	Zn(II) complex
Absorption	Water solubility	-2.422	-2.892	-2.892	-2.892	-2.892
	Intestinal absorption (human)	90.063	89.314	89.304	89.295	89.393
	Skin Permeability	-2.735	-2.735	-2.735	-2.735	-2.735
Distribution	VDSS (human)	0.063	0.087	0.087	0.087	0.087
	Fraction unbound (human)	0.21	0.331	0.331	0.331	0.331
	BBB permeability	0.454	-2.422	-2.421	-2.421	-2.424
	CNS permeability	-3.192	-1.92	-1.92	-1.92	-1.92
Metabolism	CYP2D6 substrate	NO	NO	NO	NO	NO
	CYP3A4 substrate	NO	YES	YES	YES	YES
	CYP1A2 inhibitor	YES	NO	NO	NO	NO
	CYP2C19 inhibitor	NO	YES	YES	YES	YES
Excretion	Total clearance	0.615	1.56	1.548	1.549	1.411
	Renal OCT2 substrate	NO	YES	YES	YES	YES
Toxicity	AMES toxicity	YES	NO	NO	NO	NO
	Max. tolerated dose (human)	0.681	0.411	0.411	0.411	0.411
	HERG I inhibitor	NO	NO	NO	NO	NO
	HERG II inhibitor	NO	YES	YES	YES	YES
	Oral rat acute toxicity (LD50)	2.628	2.481	2.481	2.481	2.481
	Oral rat chronic toxicity (LOAEL)	1.25	-0.15	-0.15	-0.149	-0.153
	Hepatotoxicity	YES	NO	NO	NO	NO
	Skin sensitisation	NO	NO	NO	NO	NO
	T. pyriformis toxicity	0.285	0.285	0.285	0.285	0.285
	Minnow toxicity	1.539	-2.013	-2.007	-2.001	-2.065

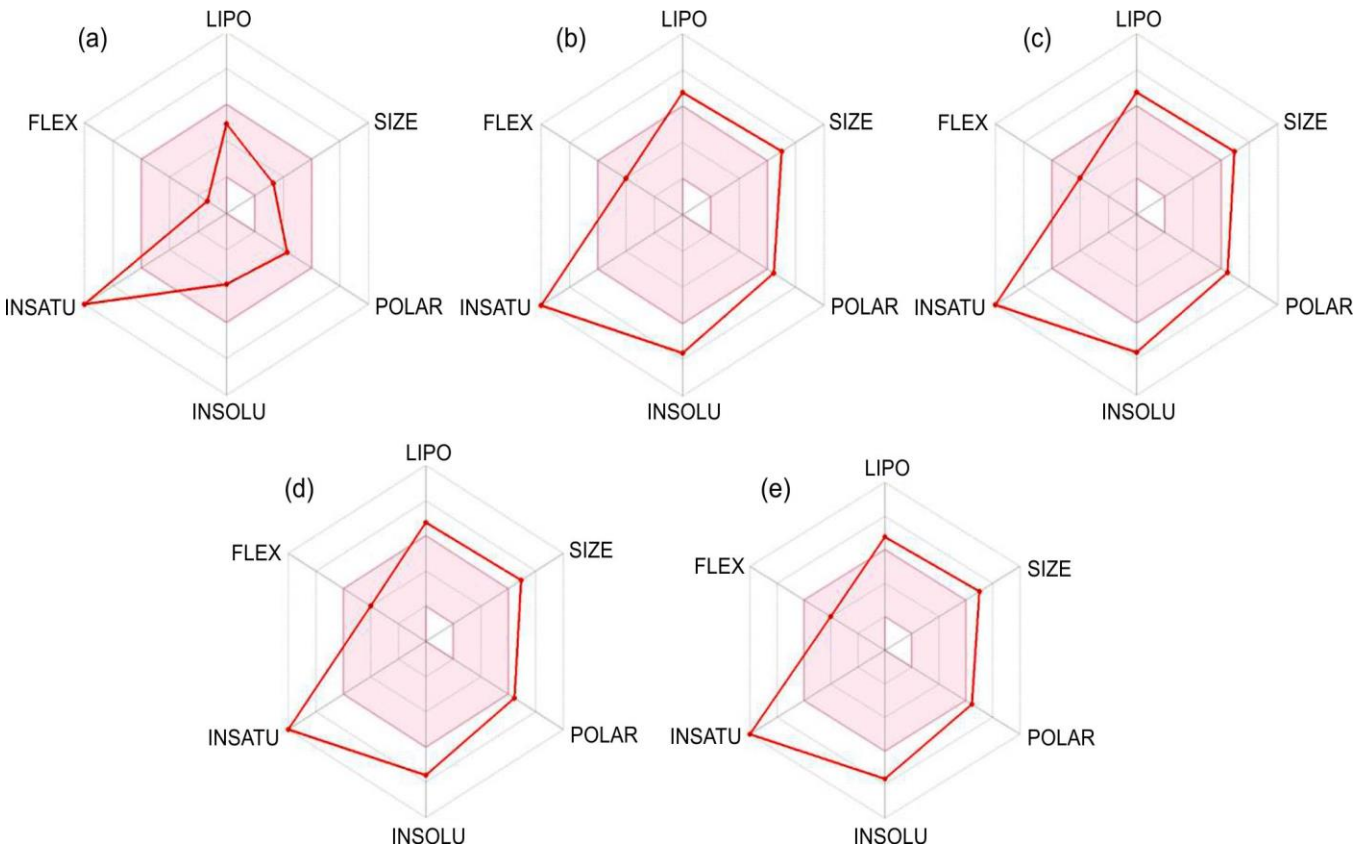

Fig. 5. Bioavailability radar to show the drug similarity of imidazole-Based Schiff base ligand and its metal(II) complexes

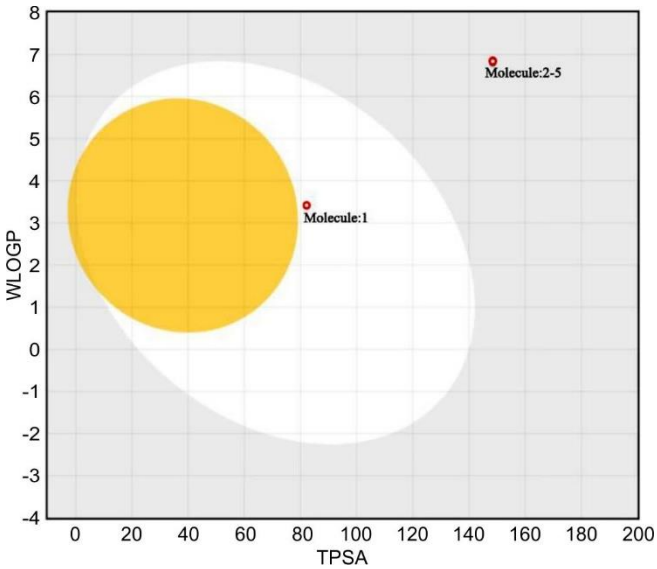

Fig. 6. BOILED-egg model of the TC for the prediction of BBB and GI activity

within the white region, suggesting a high likelihood of passive gastrointestinal absorption, while remaining outside the BBB-permeable region. Moreover, the ligand exhibited a negative P-glycoprotein profile, indicating a lower probability of active efflux, which may enhance its oral bioavailability. These features are particularly advantageous for orally administered therapeutic agents.

Prediction of activity spectra for substances (PASS) online: PASS online analysis revealed that both the Schiff base ligand and its corresponding metal(II) complexes possess significant probabilities for several biological activities, as summarized in Table-4. In all cases, the predicted probabilities of activity (Pa) exceeded those of inactivity (Pi), indicating potential bioactivity of the investigated compounds.

The free ligand exhibited the highest predicted activity as a thioredoxin inhibitor (Pa = 0.564), surpassing the corresponding metal complexes, suggesting that metal coordination slightly modulates this activity [35]. Among the metal(II) complexes, the Co(II) derivative showed the highest predicted anti-Parkinsonian potential (Pa = 0.636), implying an enhancement of this activity upon cobalt coordination. Moderate anti-Parkinsonian activity was also predicted for the Cu(II), Ni(II) and Zn(II) complexes.

Antineoplastic (melanoma) activity was predicted for both the Schiff base ligand and the metal(II) complexes with comparable Pa values, indicating retention of anticancer potential following metal coordination. In contrast, analgesic and antimitotic activities were predicted only for the free ligand, suggesting that these activities are attenuated upon the complex formation. Overall, the PASS predictions highlight the multifunctional bioactivity of the Schiff base ligand and demonstrate the role of metal coordination in modulating specific biological responses, supporting further experimental evaluation.

Molecular properties and drug-likeness prediction: The drug-likeness of the Schiff base ligand and its metal(II) complexes was evaluated using the Molsoft LLC platform and the calculated physico-chemical parameters are summarized in Table-5. The analysis is based on the drug-likeness model score, where positive values indicate drug-like behaviour and negative values suggest non-drug-like characteristics.

TABLE-4
PROBABLE ACTIVITY SPECTRUM OF SCHIFF BASE LIGAND AND ITS METAL(II) COMPLEXES AS OBTAINED FROM ONLINE SOFTWARE PASS ONLINE

Activity	Imidazole		Cu(II) complex		Co(II) complex		Ni(II) complex		Zn(II) complex	
	Pa	Pi	Pa	Pi	Pa	Pa	Pa	Pi	Pa	Pi
Thioredoxin inhibitor	0.564	0.038	0.483	0.064	0.483	0.064	0.483	0.064	0.446	0.079
Antineoplastic (melanoma)	0.294	0.023	0.341	0.016	0.341	0.016	0.341	0.016	0.289	0.024
Antimitotic	0.386	0.014	–	–	–	–	–	–	–	–
Analgesic	0.279	0.143	–	–	–	–	–	–	–	–
Antiparkinsonian	0.504	0.012	0.449	0.036	0.636	0.005	0.449	0.019	0.386	0.032
Antihelmintic	0.332	0.029	0.246	0.060	0.246	0.060	0.246	0.060	0.209	0.057
Antineoplastic (melanoma)	0.294	0.023	0.341	0.016	0.341	0.016	0.341	0.016	0.289	0.024

TABLE-5
PHYSICO-CHEMICAL PROPERTIES, DRUG-LIKENESS AND DRUG-LIKENESS SCORES OF SCHIFF BASES AND ITS COMPLEXES

Properties	Schiff base ligand	Cu(II) complex	Co(II) complex	Ni(II) complex	Zn(II) complex
Molecular formula	$C_{11}H_7N_4SCl$	$C_{22}H_{14}CuN_8S_2Cl_2$	$C_{22}H_{14}CoN_8S_2Cl_2$	$C_{22}H_{14}NiN_8S_2Cl_2$	$C_{22}H_{14}ZnN_8S_2Cl_2$
Molecular weight	262.01	586.95 (> 500)	582.95 (> 500)	581.95 (> 500)	587.95 (> 500)
Number of HBA	4	6	8	8	6
Number of HBD	1	2	2	2	2
MolLogP	2.81	5.37 (> 5)	5.41 (> 5)	5.41 (> 5)	5.37 (> 5)
MolLogS	-3.62 (Log(mol/L)) 62.46 (mg/L)	-6.22 (Log(mol/L)) 0.35 (mg/L)	-6.24 (Log(mol/L)) 0.33 (mg/L)	-6.24 (Log(mol/L)) 0.33 (mg/L)	-6.22 (Log(mol/L)) 0.35 (mg/L)
MolPSA	40.34 A^2	65.39 A^2	80.17 A^2	80.17 A^2	57.29 A^2
Molvol	219.63 A^3	450.70 A^3	427.31 A^3	429.51 A^3	449.83 A^3
PKa of most basic/acidic group	5.61/14.18	0.60/14.32	5.61/14.18	5.61/14.18	0.60/14.32
Number of stereo centers	0	0	0	0	0
Drug-likeness model score	0.29	-0.45	-0.47	-0.47	-0.45

The Schiff base ligand exhibited a positive drug-likeness score (0.29), confirming its favourable drug-like nature. This observation is supported by its moderate molecular weight, acceptable lipophilicity (MolLogP = 2.81), suitable polar surface area and compliance with key drug-likeness criteria. In contrast, all the metal(II) complexes showed negative drug-likeness scores (-0.45 to -0.47), primarily attributed to their higher molecular weights (>500 Da), increased lipophilicity (MolLogP > 5), reduced solubility and larger molecular volumes. Despite the reduced drug-likeness scores of the metal complexes, their physico-chemical profiles remain relevant for bioactivity, particularly in non-oral or targeted therapeutic applications. The graphical representation in Fig. 7 further highlights the clear distinction between the Schiff base ligand and its metal(II) complexes in terms of drug-likeness scores, emphasizing the impact of metal coordination on physico-chemical properties and oral drug-likeness [36].

Molecular docking: Molecular docking studies were conducted to assess the binding affinities of the Schiff base ligand and its metal(II) complexes toward the antioxidant proteins 1HD2 and 1FHA. The free ligand exhibited moderate binding toward 1HD2 (-4.9 kcal/mol), whereas all metal(II) complexes showed enhanced affinities, with Zn(II) complex displaying the strongest interaction (-6.1 kcal/mol), followed by Cu(II) (-6.0 kcal/mol), Ni(II) (-6.0 kcal/mol) and Co(II) (-5.9 kcal/mol) complexes. A similar trend was observed for the 1FHA target, where the ligand showed moderate binding (-5.5 kcal/mol), while the metal coordination significantly improved interaction strength. Notably, the Cu(II) complex exhibited the highest binding affinity toward 1FHA (-7.9 kcal/mol), followed by the Zn(II) complex (-7.7 kcal/mol), with the Co(II) and Ni(II) complexes showing comparable affinities (-6.4 kcal/mol). These results demonstrate that metal complexation enhances the binding efficiency of Schiff base ligand toward antioxidant targets, supporting the improved antioxidant potential of the synthesized metal(II) complexes [37]. The corresponding docking interaction poses are illustrated in Figs. 8-13 [37].

Furthermore, the Schiff base ligand and its metal(II) complexes were also evaluated for their interaction with the antidiabetic protein, mammalian pancreatic α-amylase (PDB ID: 2QV4). The ligand alone showed a moderate binding score of -6.8 kcal/mol. Upon metal complexation, the binding scores improved for all metal(II) complexes. The Co(II) complex exhibited the highest binding score of -7.7 kcal/mol, followed by Cu(II), Ni(II) and Zn(II) complexes, each displaying similar binding scores of -7.4 kcal/mol. The docking interaction images between the protein, the Schiff base ligand and its metal(II) complexes are shown in Figs. 14-16.

In vitro biological activities

Antioxidant activities: Among the metal (II) complexes, Zn(II) complex emerged as the most potent antioxidant in all three investigated assays. In the FRAP assay, Zn(II) complex demonstrated the highest ferric ion reduction with the value of 22.05 μg mL^{-1}, outperforming the other metal ions and showing antioxidant activity comparable to that of ascorbic acid. The ABTS assay also revealed the Zn(II) complex with 25.31% as the most effective at scavenging the ABTS radical cation, with its activity surpassing that of the Schiff base ligand, Cu(II), Co(II) and Ni(II) complexes. Furthermore, in the DPPH assay, the Zn(II) complex exhibited the strongest free radical scavenging activity, with an IC_{50} value of 12.64 lower than those of the other compounds as well as standard, reinforcing its superior antioxidant potential. These results highlight the Zn(II) complex as a highly effective antioxidant across all three methods tested and it is in the order of Zn^{2+} > Co^{2+} > Cu^{2+} > Ni^{2+} > Schiff base ligand, as shown in Table-6.

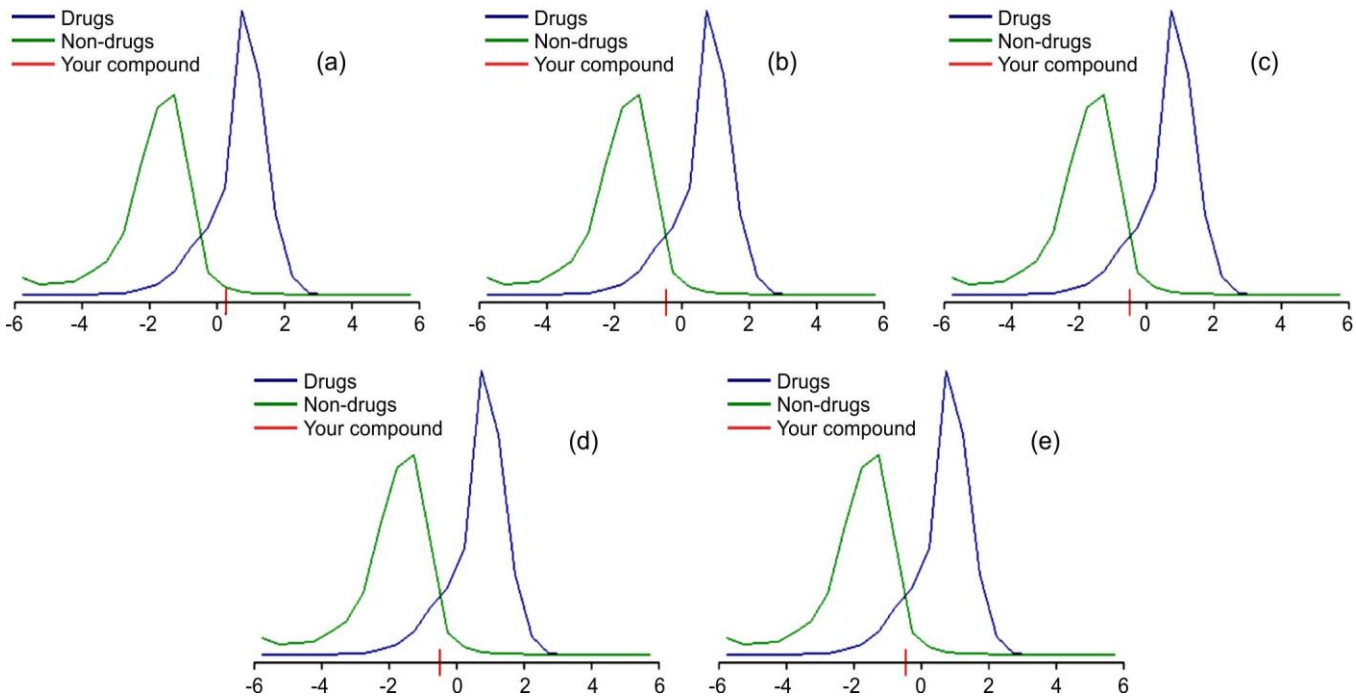

Fig. 7. The drug-likeness model scores of the Schiff base ligand and its metal(II) complexes

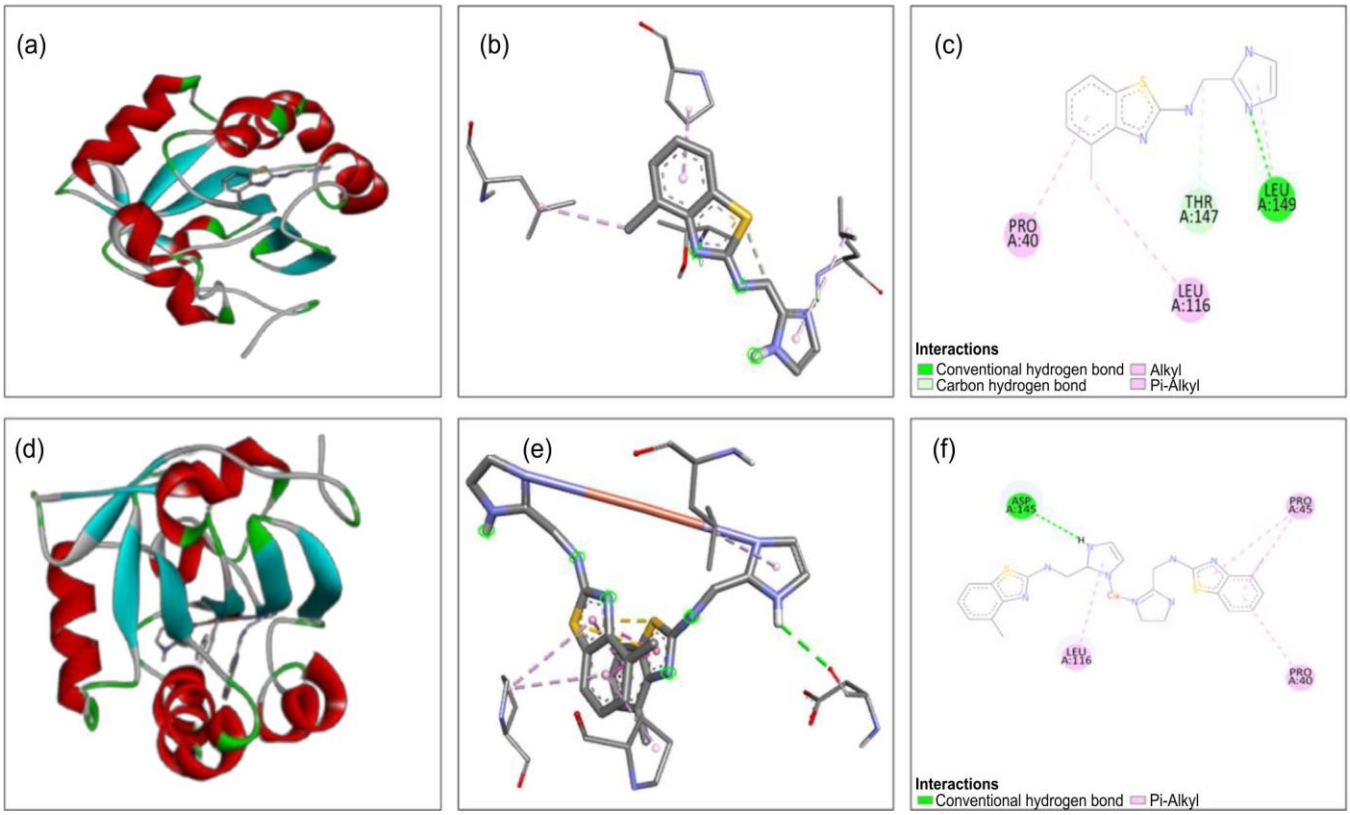

Fig. 8. Protein-ligand complex of Schiff base ligand with the active site of 1HD2 (a & b), molecular docking 2D interaction of ligand (c). Protein-ligand complex of Cu(II) with the active site of 1HD2 (d & e) molecular docking 2D interaction of Cu(II) (f)

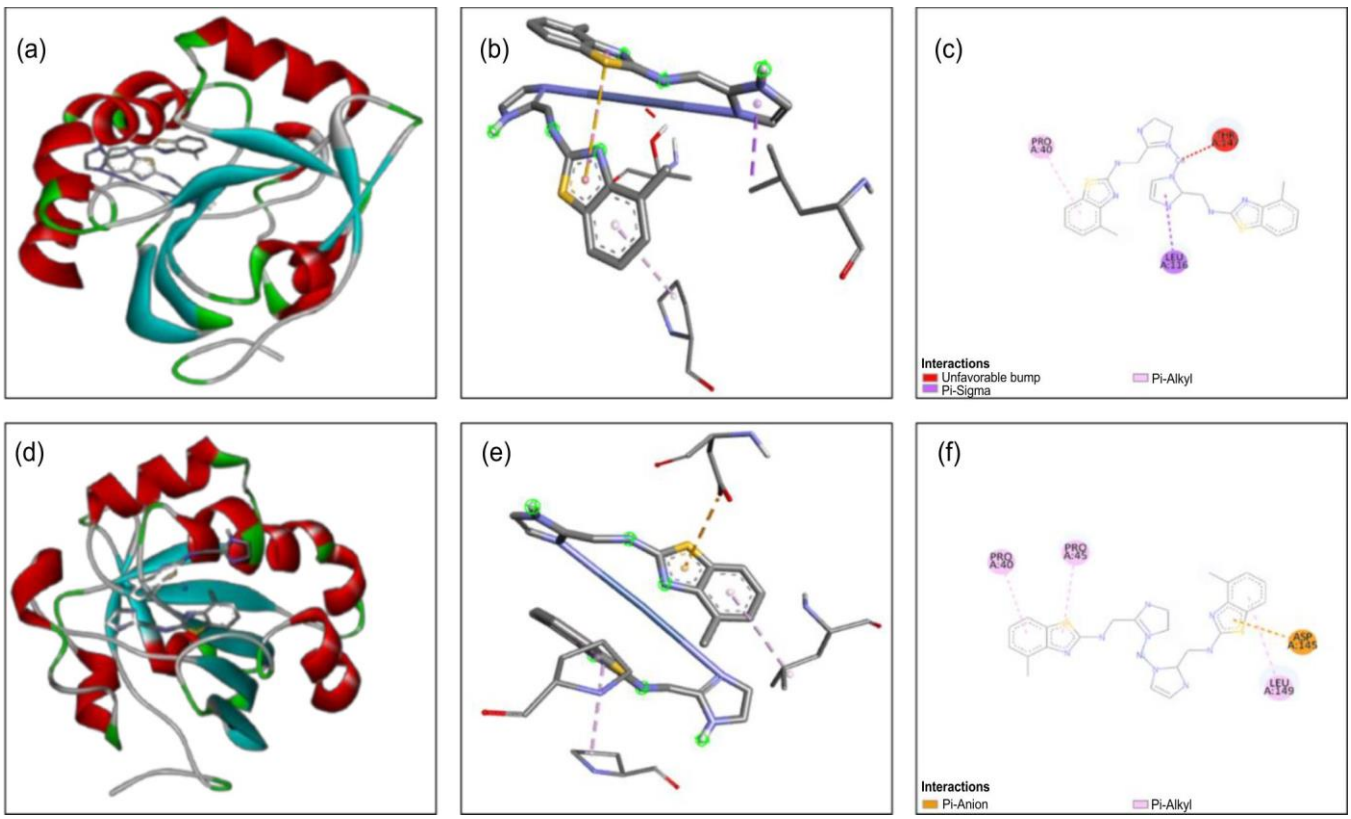

Fig. 9. Protein-ligand complex of Co(II) with the active site of 1HD2 (a & b), molecular docking 2D interaction of Co(II) (c). Protein-ligand complex of Ni(II) with the active site of 1HD2 (d & e) molecular docking 2D interaction of Ni(II) (f)

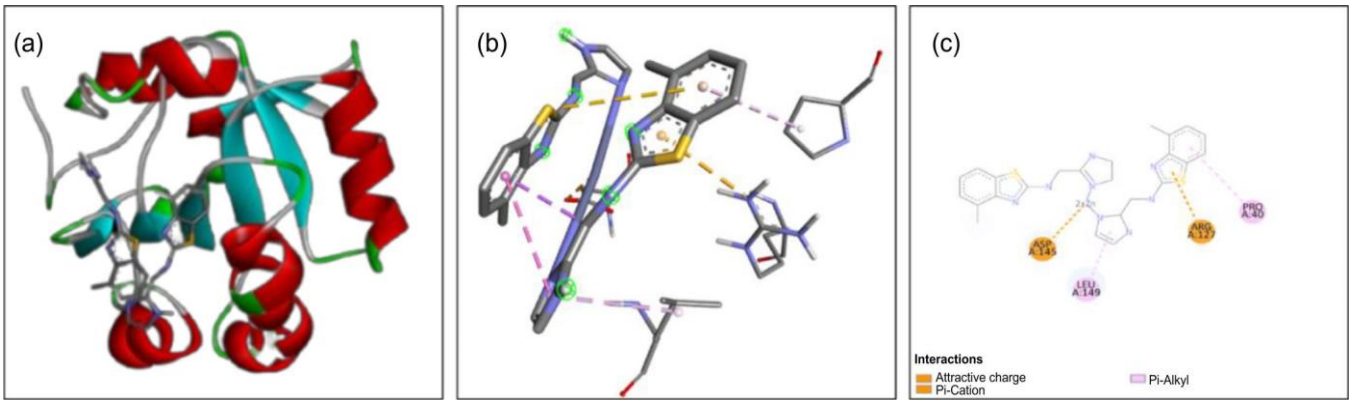

Fig. 10. Protein-ligand complex of Zn(II) with the active site of 1HD2 (a & b), molecular docking 2D interaction of Zn(II) (c)

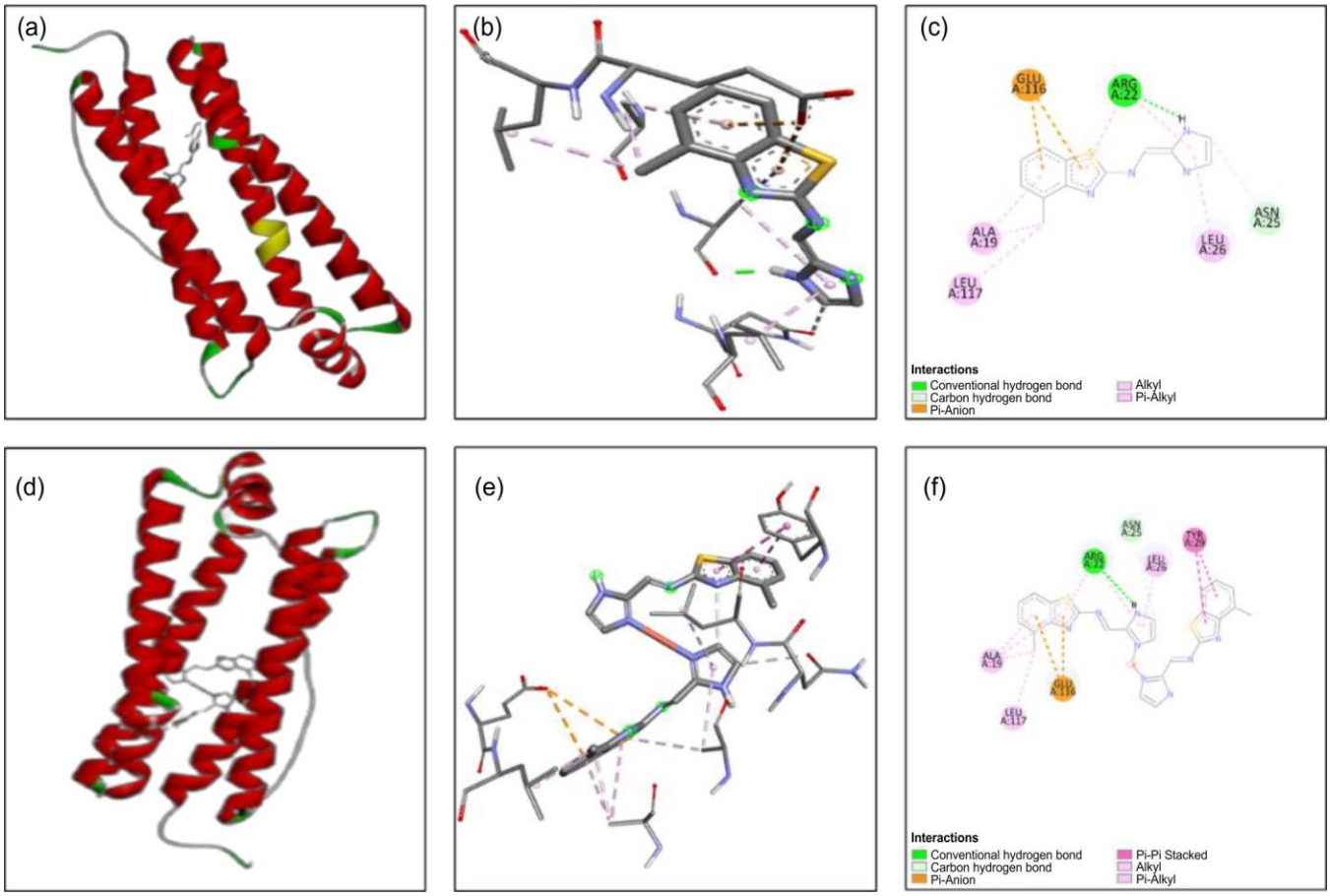

Fig. 11. Protein-ligand complex of Schiff base ligand with the active site of 1FHA (a & b), molecular docking 2D interaction of ligand (c). Protein-ligand complex of Cu(II) with the active site of 1FHA (d & e) molecular docking 2D interaction of Cu(II) (f)

TABLE-6
BIOLOGICAL ACTIVITIES DATA OF IMIDAZOLE-BASED SCHIFF BASE LIGAND AND ITS METAL(II) COMPLEXES

Compounds	Antioxidant activities			Anti-diabetic activity
	IRP (μg mL^{-1})	ABTS (%)	DPPH (IC_{50} μg mL^{-1})	α-Amylase enzyme inhibition (%)
Schiff base ligand	35.26	45.31	16.35	38.68
Cu(II) complex	25.36	27.35	13.65	32.38
Co(II) complex	24.01	26.31	13.54	30.24
Ni(II) complex	25.98	32.50	13.98	34.68
Zn(II) complex	22.05	25.31	12.64	30.36
Ascorbic acid	–	40.05	3.98	–
Acarbose	–	–	–	50.35

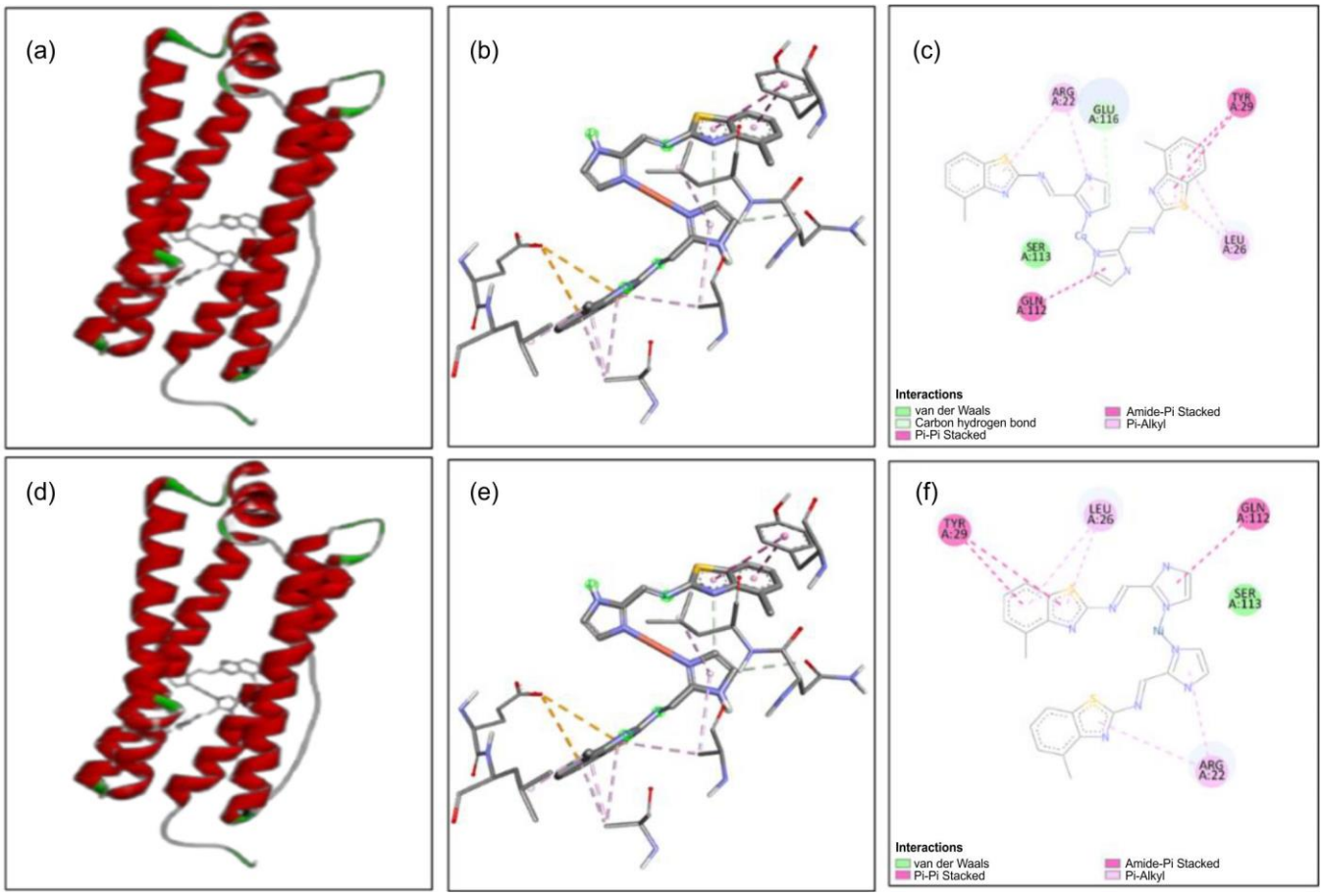

Fig. 12. Protein-ligand complex of Co(II) with the active site of 1FHA (a & b), molecular docking 2D interaction of Co(II) (c). Protein-ligand complex of Ni(II) with the active site of 1FHA (d & e) molecular docking 2D interaction of Ni(II) (f)

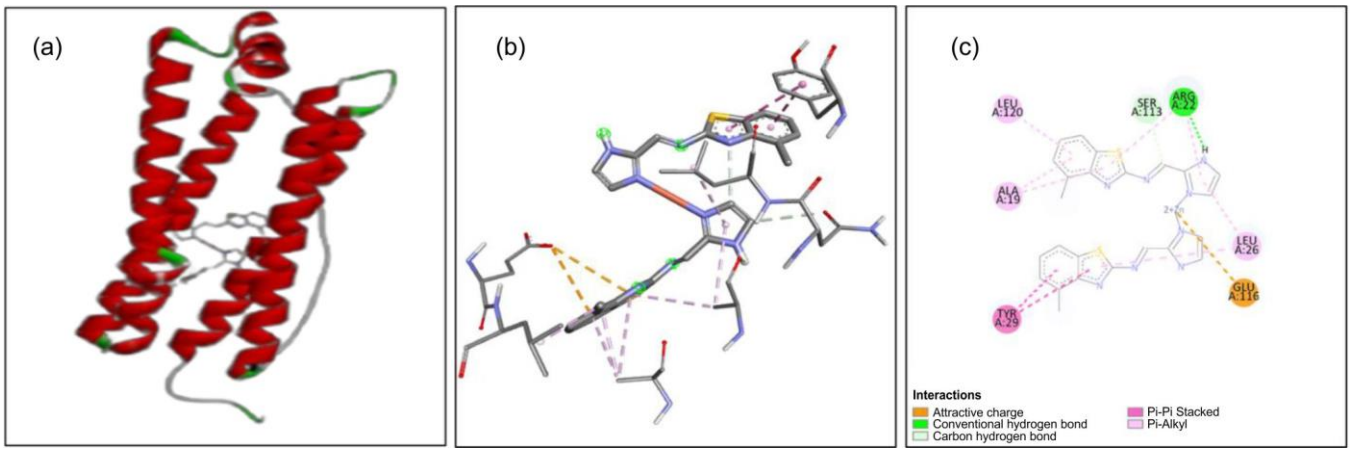

Fig. 13. Protein-ligand complex of Zn(II) with the active site of 1FHA (a & b), molecular docking 2D interaction of Zn(II) (c)

Antidiabetic activity: Among the Schiff base metal(II) complexes, the Co(II) complex emerged as the most potent inhibitor of α-amylase activity, outperforming the other metal(II) complexes and showing the highest inhibitory effect. In comparison to standard acarbose, a standard α-amylase inhibitor, the Co(II) complex demonstrated a similar or slightly stronger inhibitory activity, with its IC_{50} value of 26.31 comparable to that of acarbose and all other compounds. This suggests that the Co(II) complex is highly effective in modulating α-amylase activity, making it a promising candidate for further exploration as a potential therapeutic agent for managing conditions related to carbohydrate metabolism. The order of activity can be shown as follows: $Co^{2+} > Zn^{2+} > Cu^{2+} > Ni^{2+}$ > Schiff base ligand, as presented in Table-6.

Conclusion

The synthesis and characterisation of Cu(II), Co(II), Ni(II) and Zn(II) transition metal complexes with the imidazole-

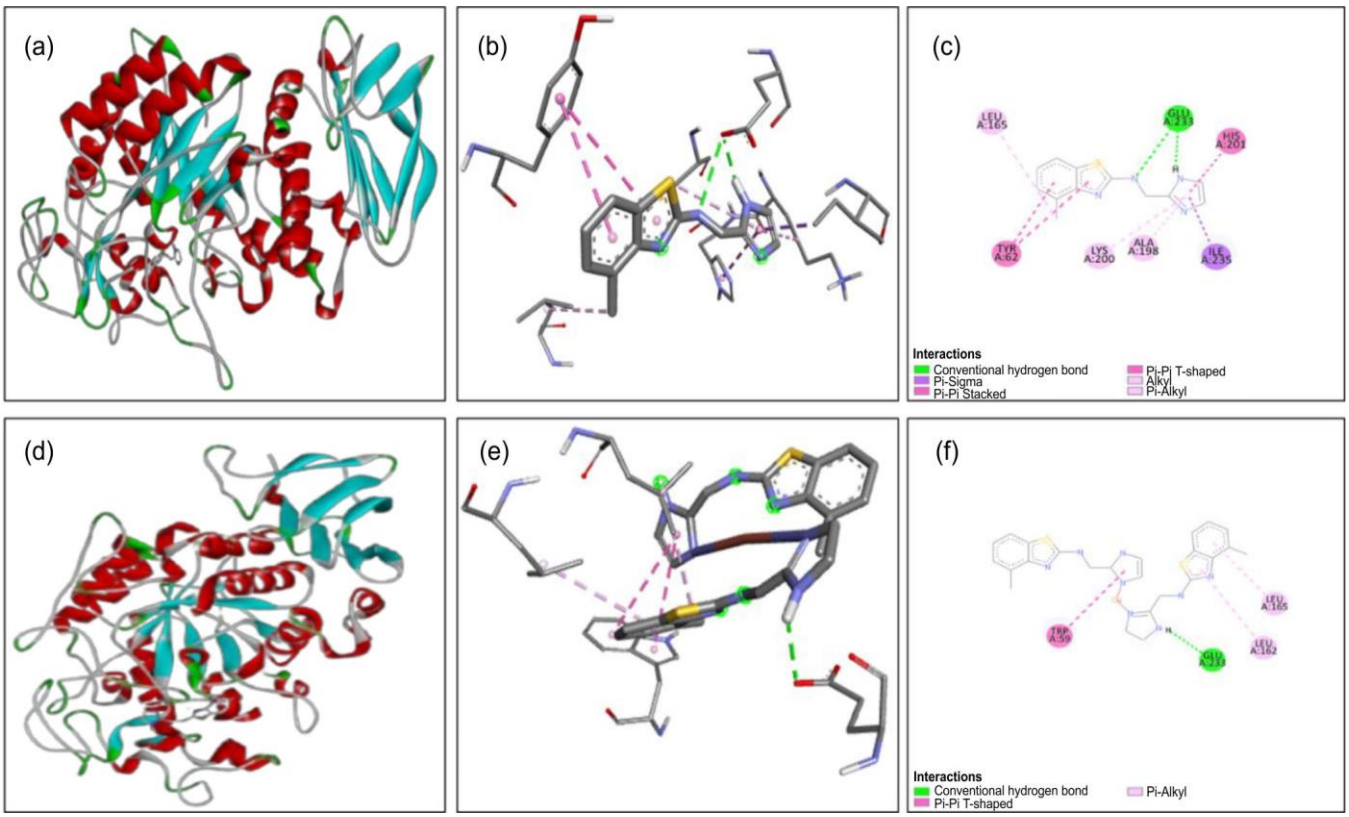

Fig. 14. Protein-ligand complex of Schiff base ligand with the active site of 2QV4 (a & b), molecular docking 2D interaction of ligand (c). Protein-ligand complex of Cu(II) with the active site of is 2QV4 (d & e) molecular docking 2D interaction of Cu(II) (f)

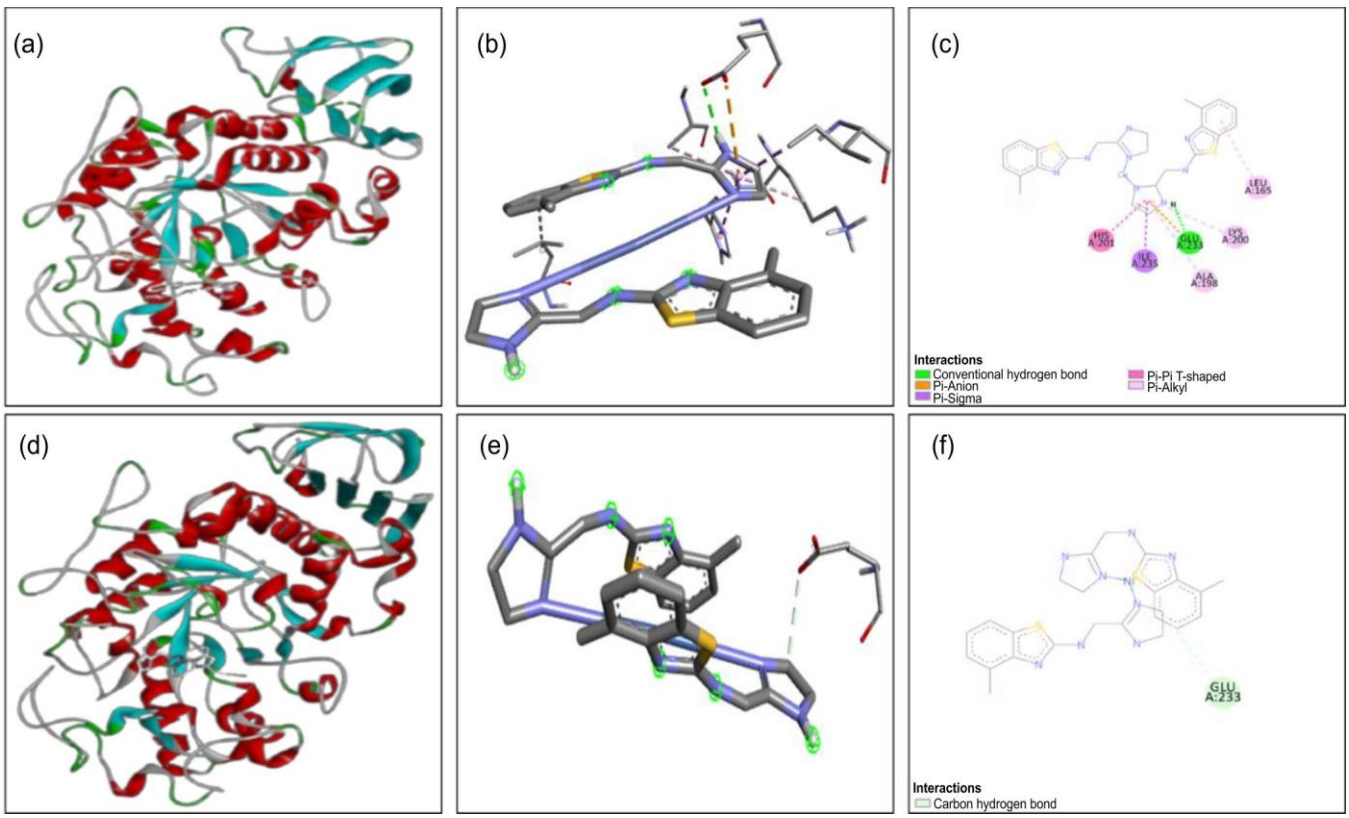

Fig. 15. Protein-ligand complex of Co(II) with the active site of 2QV4 (a & b), molecular docking 2D interaction of Co(II) (c). Protein-ligand complex of Ni(II) with the active site of 2QV4 (d & e) molecular docking 2D interaction of Ni(II) (f)

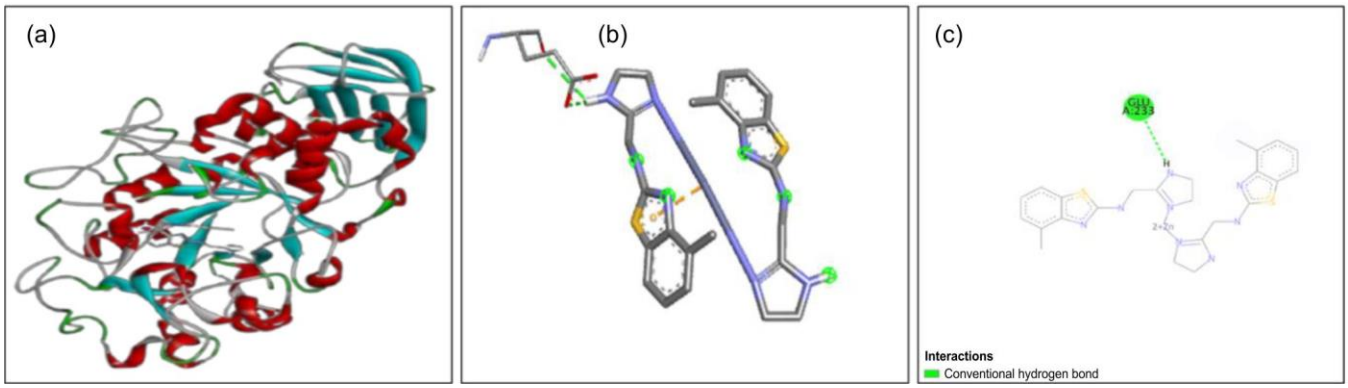

Fig. 16. Protein-ligand complex of Zn(II) with the active site of 2QV4 (a & b), molecular docking 2D interaction of Zn(II) (c)

based Schiff base ligand, (*E*)-*N*-(4-chlorobenzo[*d*]thiazol-2-yl)-1-(1*H*-indole-3-yl)methanimine, demonstrated promising structural and coordination features. Spectroscopic analyses, including mass, NMR and FT-IR, confirmed the successful coordination of the Schiff base ligand with the transition metal(II) ions. The physico-chemical properties, drug-likeness and pharmacokinetic profiles predicted through the Swiss ADME web server highlighted the compounds' potential as drug candidates. Moreover, the bioactivity predictions from PASS analysis reinforced the therapeutic promise of both the Schiff base ligand and its metal(II) complexes. Molecular docking studies further supported these findings. The Schiff base ligand and its metal(II) were evaluated for their binding affinity with the antioxidant protein 1HD2. The ligand alone showed a moderate binding score of -4.9 kcal/mol, while the metal complexes exhibited higher binding affinities. The Zn(II) complex showed the highest binding score of -6.1 kcal/mol, followed by Cu(II) (-6.0 kcal/mol), Ni(II) (-6.0 kcal/mol) and Co(II) (-5.9 kcal/mol), suggesting that metal complexation enhances the ligand's antioxidant properties. The antioxidant activity, evaluated through the FRAP, ABTS and DPPH assays, demonstrated that the Zn(II) complex exhibited the most potent antioxidant activity, outperforming the other metal(II) complexes and showing comparable or superior results to ascorbic acid. Furthermore, the Co(II) complex emerged as the most effective inhibitor of α-amylase activity among the metal complexes, with a potency similar to that of the standard inhibitor, acarbose, exhibiting its potential for antidiabetic applications. These results collectively underscore the promising therapeutic potential of these metal-ligand complexes for both antioxidant and antidiabetic applications.

ACKNOWLEDGEMENTS

The authors express their sincere gratitude to TEQIP-III, National Project Implementation Unit (NPIU), Sri Jayachamarajendra College of Engineering and JSS Science and Technology University, Mysuru, for their financial support and for providing the necessary instrumentation facilities.

CONFLICT OF INTEREST

The authors declare that there is no conflict of interests regarding the publication of this article.

DECLARATION OF AI-ASSISTED TECHNOLOGIES

During the preparation of this manuscript, the authors used an AI-assisted tool(s) to improve the language. The authors reviewed and edited the content and take full responsibility for the published work.

REFERENCES

1. C. Boulechfar, H. Ferkous, A. Delimi, A. Djedouani, A. Kahlouche, A. Boublia, A.S. Darwish, T. Lemaoui, R. Verma and Y. Benguerba, *Inorg. Chem. Commun.*, **150**, 110451 (2023); https://doi.org/10.1016/j.inoche.2023.110451
2. M. Pervaiz, R. Quratulain, A. Ejaz, M. Shahin, Z. Saeed, S. Nasir, R. Rashad Mahmood Khan, A. Ashraf, S. Ullah and U. Younas, *Inorg. Chem. Commun.*, **160**, 111856 (2024); https://doi.org/10.1016/j.inoche.2023.111856
3. R. Malav and S. Ray, *RSC Adv.*, **15**, 22889 (2025); https://doi.org/10.1039/D5RA03626G
4. N. Nidhi, Siddharam, D.P. Rao, A.K. Gautam, A. Verma and Y. Gautam, *Results Chem.*, **13**, 101941 (2025); https://doi.org/10.1016/j.rechem.2024.101941
5. K. Brodowska and E. Łodyga-Chruścińska, *Chemik*, **68**, 129 (2014).
6. K. Jomova, M. Makova, S.Y. Alomar, S.H. Alwasel, E. Nepovimova, K. Kuca, C.J. Rhodes and M. Valko, *Chem. Biol. Interact.*, **367**, 110173 (2022); https://doi.org/10.1016/j.cbi.2022.110173
7. D. Karati, S. Mukherjee and S. Roy, *Med. Chem.*, **19**, 960 (2023); https://doi.org/10.2174/1573406419666230707105221
8. X. Liu and J.R. Hamon, *Coord. Chem. Rev.*, **389**, 94 (2019); https://doi.org/10.1016/j.ccr.2019.03.010
9. S. Kumar, A. Arora, V.K. Maikhuri, A. Chaudhary, R. Kumar, V.S. Parmar, B.K. Singh and D. Mathur, *RSC Advances*, **14**, 17102 (2024); https://doi.org/10.1039/D4RA00590B
10. B. Gowdhami, S. Ambika, B. Karthiyayini, V. Ramya, B. Kadalmani, R.T.V. Vimala and M.A. Akbarsha, *Toxicol. In Vitro*, **75**, 105201 (2021); https://doi.org/10.1016/j.tiv.2021.105201
11. S. Yadav, S.P. Sonkar, K.S. Tiwari and M. Shukla, *Results Chem.*, **10**, 101743 (2024); https://doi.org/10.1016/j.rechem.2024.101743
12. M. Stradiotto and R.J. Lundgren, Eds., Key Concepts in Ligand Design: An Introduction, In: Ligand Design in Metal Chemistry: Reactivity and Catalysis, edn. 1, Chap. 1, pp. 1-14, John Wiley & Sons, Ltd. (2016).
13. S. Mondal, S.M. Mandal, T.K. Mondal and C. Sinha, *J. Mol. Struct.*, **1127**, 557 (2017); https://doi.org/10.1016/j.molstruc.2016.08.011
14. P. Durairaj, T. Maruthavanan, S. Manjunathan, S. Subashini, S.L. Rokhum and G. Baskar, *J. Mol. Struct.*, **1295**, 136650 (2024); https://doi.org/10.1016/j.molstruc.2023.136650

15. S. Paul, H.P. Gogoi, A. Singh and P. Barman, *Inorg. Chem. Commun.*, **153**, 110760 (2023); https://doi.org/10.1016/j.inoche.2023.110760
16. F.A. Almalki, A.N. Abdalla, A.M. Shawky, M.A. El Hassab and A.M. Gouda, *Molecules*, **26**, 4002 (2021); https://doi.org/10.3390/molecules26134002
17. S. Maddikayala, K. Bengi, V. Malkhed and S.R. Pulimamidi, *Appl. Organomet. Chem.*, **39**, e7949 (2025); https://doi.org/10.1002/aoc.7949
18. S. Şahin and N. Dege, *J. Mol. Struct.*, **1250**, 131744 (2022); https://doi.org/10.1016/j.molstruc.2021.131744
19. P. Jeyaraman, S. Michael, R. Natrajan and A.A.R. Adaikalam, *Struct. Chem.*, **34**, 1115 (2023); https://doi.org/10.1007/s11224-022-02065-0
20. L.H. Abdel-Rahman, A.A. Abdelghani, A.A. AlObaid, D.A. El-ezz, I. Warad, M.R. Shehata and E.M. Abdalla, *Sci. Rep.*, **13**, 3199 (2023); https://doi.org/10.1038/s41598-023-29386-2
21. W.H. Mahmoud, R.G. Deghadi and G.G. Mohamed, *J. Therm. Anal. Calorim.*, **127**, 2149 (2017); https://doi.org/10.1007/s10973-016-5826-7
22. T. Alorini, I. Daoud, A.N. Al-Hakimi and F. Alminderej, *J. Mol. Struct.*, **1276**, 134785 (2023); https://doi.org/10.1016/j.molstruc.2022.134785
23. M. Ibrahim, A. Khan, M. Ikram, S. Rehman, M. Shah, H. Nabi and A. Ahuchaogu, *Asian J. Chem. Sci*, **2**, 1 (2017); https://doi.org/10.9734/AJOCS/2017/32244
24. E. Bursal, F. Turkan, K. Buldurun, N. Turan, A. Aras, N. Çolak, M. Murahari and M.C. Yergeri, *Biometals*, **34**, 393 (2021); https://doi.org/10.1007/s10534-021-00287-z
25. N.H. Boukoucha, Z. Messasma, D. Aggoun, Y. Ouennoughi, C. Bensouici, M. Fernández-García, D. Lopez, M. Guelfi, F. Marchetti, G. Bresciani and Z. Chorfi, *J. Mol. Struct.*, **1319**, 139505 (2025); https://doi.org/10.1016/j.molstruc.2024.139505
26. Y. Deswal, S. Asija, A. Dubey, L. Deswal, D. Kumar, D. Kumar Jindal and J. Devi, *J. Mol. Struct.*, **1253**, 132266 (2022); https://doi.org/10.1016/j.molstruc.2021.132266
27. S. Zehra, M. Shavez Khan, I. Ahmad and F. Arjmand, *J. Biomol. Struct. Dyn.*, **37**, 1863 (2019); https://doi.org/10.1080/07391102.2018.1467794
28. V.H. Mariswamy, D. Puttaveerappa, S.K. Prasad, C. Shivamallu, R. Veerapur, S.R. Prasad et al., (2020). Chemical Synthesis, Spectral Characterization and Antitumor Activity of Co (II), Zn (II) and Ni (II) Complexes Derived from Thiazole-based Schiff Base Ligand.
29. Puttaveerappa, D., Marisamy, V. H., Begum, M., Ramu, R., Shirahatti, P. S., Prasad, N., & Dharmappa, R. N. (2024). Preparation, Characterization, and Biological Activity of Cu (II) and Co (II) Complexes of 5-(((E)-3-Phenylallylidene) Amino-1, 3, 4-Thiadaizole-2-Thiol Schiff Base Ligand.
30. P. Deepika, H.M. Vinusha, M. Begum, R. Ramu, P.S. Shirahatti and M.N. Nagendra Prasad, *Heliyon*, **8**, e09648 (2022); https://doi.org/10.1016/j.heliyon.2022.e09648
31. E.S. Aazam, A.F. EL Husseiny and H.M. Al-Amri, *Arab. J. Chem.*, **5**, 45 (2012); https://doi.org/10.1016/j.arabjc.2010.07.022
32. M. Türkmenoğlu, S.T. Yıldırım, A. Altay and B. Türkmenoğlu, *ChemistrySelect*, **9**, e202303519 (2024); https://doi.org/10.1002/slct.202303519
33. A. Tahmasbi, A. Jafari and A. Nikoo, *Sci. Rep.*, **13**, 10988 (2023); https://doi.org/10.1038/s41598-023-38086-w
34. Y.M.A. Jamil, F.M. Al-Azab and N.A. Al-Selwi, *Eclét. Quím.*, **48**, 36 (2023); https://doi.org/10.26850/1678-4618eqj.v48.3.2023.p36-53
35. M.I. Alam, M.A. Alam, O. Alam, A. Nargotra, S.C. Taneja and S. Koul, *Eur. J. Med. Chem.*, **114**, 209 (2016); https://doi.org/10.1016/j.ejmech.2016.03.008
36. A.M. Abu-Dief, R.M. El-Khatib, F.S. Aljohani, S.O. Alzahrani, A. Mahran, M.E. Khalifa and N.M. El-Metwaly, *J. Mol. Struct.*, **1242**, 130693 (2021); https://doi.org/10.1016/j.molstruc.2021.130693
37. J. Devi, S. Kumar, B. Kumar, S. Asija and A. Kumar, *Res. Chem. Intermed.*, **48**, 1541 (2022); https://doi.org/10.1007/s11164-021-04644-y